

Neophaseic acid catabolism in the 9'-hydroxylation pathway of abscisic acid in *Arabidopsis thaliana*

Ya-Li Bai^{1,5}, Xiaoming Yin^{1,5}, Cai-Feng Xiong¹, Bao-Dong Cai¹, Yan Wu², Xiao-Yun Zhang³, Zhenwei Wei¹, Tiantian Ye^{1,*} and Yu-Qi Feng^{1,4,*}

¹Department of Chemistry, Wuhan University, Wuhan 430072, P.R. China

²State Key Laboratory of Hybrid Rice, College of Life Sciences, Wuhan University, Wuhan 430072, P.R. China

³Department of Chemistry, Lanzhou University, Lanzhou 730000, P.R. China

⁴Frontier Science Center for Immunology and Metabolism, Wuhan University, Wuhan 430072, P.R. China

⁵These authors contributed equally to this article

*Correspondence: Tiantian Ye (ye_tiantian@whu.edu.cn), Yu-Qi Feng (yqfeng@whu.edu.cn)

<https://doi.org/10.1016/j.xplc.2022.100340>

ABSTRACT

Abscisic acid (ABA) hydroxylation is an important pathway for ABA inactivation and homeostasis maintenance. Here, we discover a new downstream catabolite of neophaseic acid (neoPA) in the ABA 9'-hydroxylation pathway and identify it as *epi*-neodihydrophaseic acid (*epi*-neoDPA) by comparing its accurate mass, retention time, and MSⁿ spectra with those of our chemically synthesized *epi*-neoDPA. Analyses of *Arabidopsis* seed germination and ABA-related gene expression reveal that neoPA rather than *epi*-neoDPA possesses ABA-like hormonal activity. *In vitro* enzyme activity tests of prokaryotic recombinant protein reveal that NeoPAR1 (neoPA reductase 1) identified from *Arabidopsis* converts neoPA into *epi*-neoDPA. Site-directed mutation at Tyr163 in the conserved motif of NeoPAR1 abolishes the catalytic activity of NeoPAR1. Accelerated seed germination was observed in *NeoPAR1* knockdown and knockout mutants, whereas retarded seed germination and the accumulation of *epi*-neoDPA and ABA were observed in *NeoPAR1* overexpression lines, suggesting that NeoPAR1 is involved in seed germination and maintenance of ABA homeostasis.

Keywords: abscisic acid, ABA catabolism, *epi*-neoDPA, neoPA reductase, seed germination, phaseic acid

Bai Y.-L., Yin X., Xiong C.-F., Cai B.-D., Wu Y., Zhang X.-Y., Wei Z., Ye T., and Feng Y.-Q. (2022). Neophaseic acid catabolism in the 9'-hydroxylation pathway of abscisic acid in *Arabidopsis thaliana*. *Plant Comm.* **3**, 100340.

INTRODUCTION

Abscisic acid (ABA) is a phytohormone with a sesquiterpenoid structure that plays critical roles in numerous plant physiological processes such as seed dormancy, seed germination, embryonic development, stomatal movement, and stress responses (Cutler et al., 2010; Merilo et al., 2015; Gao et al., 2016a; Shu et al., 2016; Vishwakarma et al., 2017). The concentration of ABA in plant tissues constantly fluctuates in dynamic physiological processes and under changing environmental conditions (Dong et al., 2015). Modulation of cellular ABA levels is necessary for balancing defense and growth processes in plants (Chen et al., 2020). The homeostasis of ABA is maintained by fine-tuning its biosynthesis, catabolism, and transport (Nambara and Marionpoll, 2005; Chen et al., 2020). Catabolism is an important pathway for ABA inactivation in plants and is carried out mainly through conjugation and hydroxylation (Nambara and Marionpoll, 2005). The conjugation of ABA with glucose is

mediated by the UDP glucosyltransferase family to yield ABA-glucose ester at 1-C in the side chain or ABA-glucoside at 1'-C in the ring (Loveys and Milborrow, 1981; Turečková et al., 2009). ABA hydroxylation is triggered by oxidation of one of the carbon atoms (7'-C, 8'-C, or 9'-C) in the ring structure (Nambara and Marionpoll, 2005) (Figure 1).

The 8'-hydroxylation pathway is the main route of ABA hydroxylation, in which catabolite structures, related enzymes, and biological functions have been extensively studied (Kushiro et al., 2004; Mizutani and Todoroki, 2006; Nambara and Marionpoll, 2005; Weng et al., 2016; Yin et al., 2022). In this pathway, ABA is initially catalyzed by 8'-hydroxylase and

Published by the Plant Communications Shanghai Editorial Office in association with Cell Press, an imprint of Elsevier Inc., on behalf of CSPB and CEMPS, CAS.

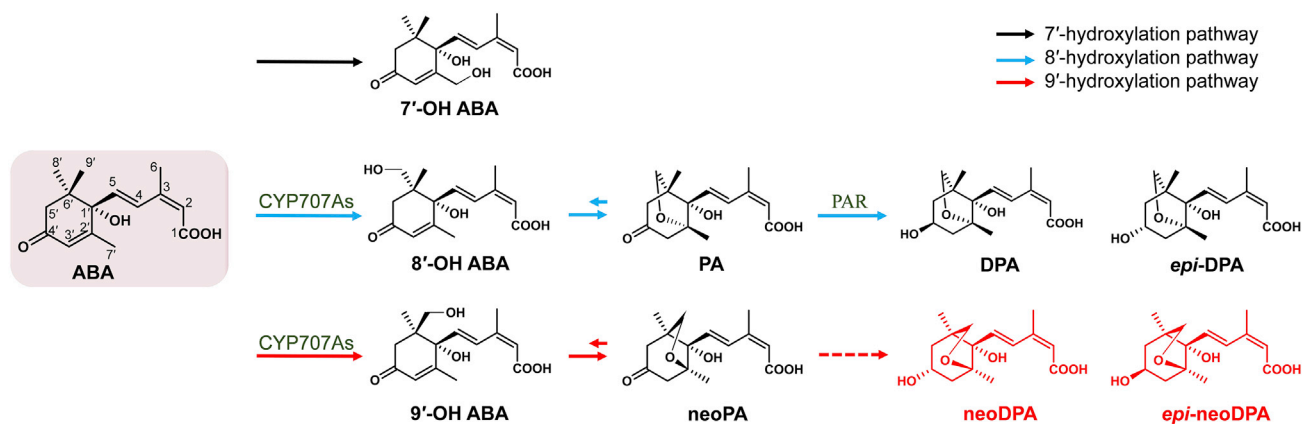


Figure 1. Partial oxidative catabolic pathways and putative downstream catabolites of ABA.

The compounds in red are putative catabolites.

converted into the unstable intermediate 8'-hydroxy ABA (8'-OH ABA) (Milborrow, 1969) (Figure 1). Then 8'-OH ABA spontaneously rearranges to generate phaseic acid (PA), and PA is further reduced by PA reductase (PAR) to form dihydrophaseic acid (DPA) and/or its analog epi-dihydrophaseic acid (*epi*-DPA) (Milborrow, 1969; Zeevaert and Milborrow, 1976). In early years, 8'-hydroxylases were reported to be a small branch of cytochrome P450 monooxygenases encoded by the CYP707A family (Kushiro et al., 2004; Mizutani and Todoroki, 2006). CYP707A genes play a key role in seed development and germination through the hydroxylation of ABA (Kushiro et al., 2004). Recently, the two PARs ABH2 (ABA hypersensitive 2) and CRL1 (cinnamoyl coA:NADP oxidoreductase like 1) from the NAD(P)-binding Rossmann-fold protein superfamily were identified and confirmed to participate in seed germination and drought tolerance in *Arabidopsis* (Weng et al., 2016; Yin et al., 2022).

In contrast to the well documented 8'-hydroxylation pathway, the 7'-hydroxylation and 9'-hydroxylation pathways of ABA are less well understood. 7'-hydroxy ABA is found in numerous plant species as a minor catabolite (Nambara and Marionpoll, 2005). The 9'-hydroxylation pathway is highly similar to the 8'-hydroxylation pathway. For instance, although these two atoms occur in different chemical environments, the 9'-C and 8'-C are both connected to the 6'-C atom of the ABA ring, and although 9'-hydroxylation is considered to be a side reaction of 8'-hydroxylation, the hydroxylations of 9'-C and 8'-C are both catalyzed by CYP707As (Chen et al., 2020). Similar to 8'-OH ABA, 9'-hydroxy ABA (9'-OH ABA) can also spontaneously rearrange into neophaseic acid (neoPA). One previous study has shown that neoPA is detected in immature seeds but not in late-development seeds, implying that it may have been metabolized (Zhou et al., 2004). However, the enzymes associated with this metabolic process and the downstream catabolites of neoPA remain unknown.

In this study, we discover a downstream catabolite of neoPA in the ABA 9'-hydroxylation pathway and identify it as *epi*-neodihydrophaseic acid (*epi*-neoDPA). Analyses of *Arabidopsis* seed germination and ABA-responsive gene expression reveal that

neoPA, rather than *epi*-neoDPA, possesses ABA-like hormonal activity. In addition, we identified a new reductase responsible for converting neoPA into *epi*-neoDPA and named it neoPA reductase 1 (NeoPAR1). Phenotypic analysis of a *NeoPAR1* transgenic line reveals that NeoPAR1 may function as a modulator in *Arabidopsis* seed germination.

RESULTS

Discovery of downstream catabolites of neoPA in the ABA 9'-hydroxylation pathway

In the ABA 8'-hydroxylation pathway, PA is reduced to DPA and *epi*-DPA. Therefore, we speculated that the downstream catabolism of neoPA in the ABA 9'-hydroxylation pathway might be similar to the catabolism of PA in the ABA 8'-hydroxylation pathway, that is, neoPA might be further reduced to neoDPA or *epi*-neoDPA (Figure 1).

It has been reported that chemical labeling can improve the detection sensitivity for plant hormones in LC-MS analysis (Yu et al., 2017; Cai et al., 2021). Therefore, in this study, *N,N*-dimethyl ethylenediamine (DMED) and *d*₄-DMED (a pair of stable isotope labeling reagents for carboxylic compounds) were used to label the extract of *Arabidopsis* siliques, as the concentration of ABA catabolites is usually very low in plant tissues (Supplemental Scheme 1). Equal amounts of DMED- and *d*₄-DMED-labeled samples were mixed and then subjected to liquid chromatography-mass spectrometry (LC-MS) analysis to obtain raw data. Afterward, features of potential neoDPA and *epi*-neoDPA were extracted from the raw data according to the expected *m/z* values of DMED- and *d*₄-DMED-labeled neoDPA/*epi*-neoDPA (353.2434 and 357.2686). Figure 2A shows the extracted ion chromatogram (EIC) of DMED- and *d*₄-DMED-labeled extract of *Arabidopsis* siliques at *m/z* of 353.2434 and 357.2686, in which two features at retention times (RTs) of 2.4 min (feature-1) and 6.8 min (feature-2) were observed. The comparison of its RT and MSⁿ spectra with those of authentic DPA standard revealed that feature-1 was DMED-DPA (Figure 2A and Supplemental Figure 1). In the MSⁿ spectra, feature-2 exhibited quite similar fragmentation patterns to DMED-DPA, but they had different RTs (Figure 2A and

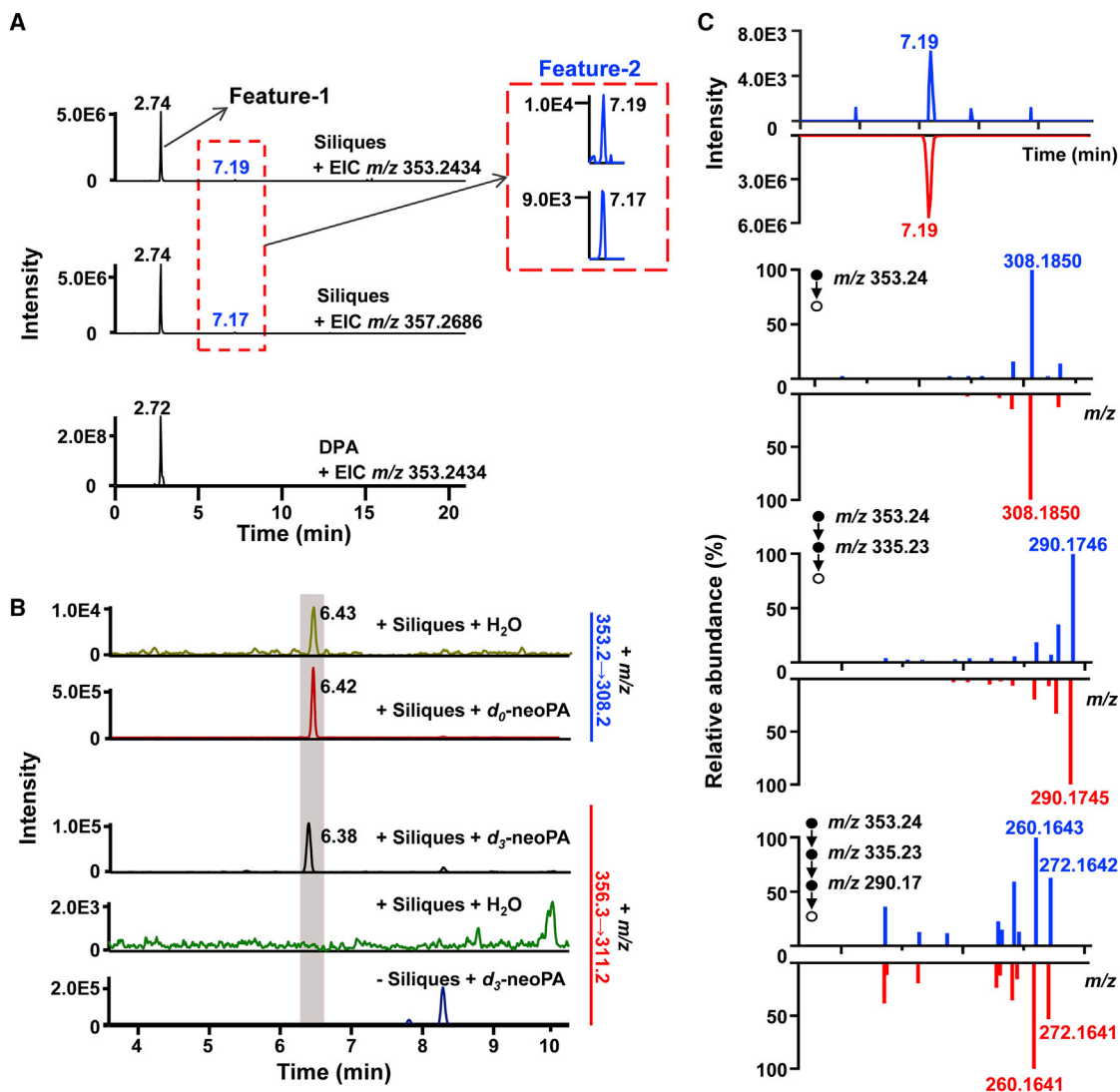


Figure 2. Discovery of downstream catabolites of neoPA in the ABA 9'-hydroxylation pathway.

(A) EIC (extracted ion chromatograms) of labeled *Arabidopsis* siliques at m/z 353.2435 (top) and m/z 357.2686 (middle) and EIC of labeled DPA standard at m/z 353.2435 (bottom).

(B) MRM (multiple reaction monitoring) chromatograms of DMED-labeled *Arabidopsis* siliques treated with H₂O (yellow) and *d*₀-neoPA (red) at m/z 353.2 → 308.2; MRM chromatogram of DMED-labeled *Arabidopsis* siliques treated with *d*₃-neoPA (black) and H₂O (green) at m/z 356.3 → 311.2; and MRM chromatogram of DMED-labeled *d*₃-neoPA at m/z 356.3 → 311.2 (blue).

(C) Identification of a discovered catabolite of neoPA (blue) in the ABA 9'-hydroxylation pathway by comparison of its RT and MSⁿ spectra with those of synthetic *epi*-neoDPA (red). Spectra in Figure 2A and 2C were obtained on an LTQ-Orbitrap Mass Spectrometer. Spectra in Figure 2B were obtained on a TSQ Quantiva Triple-Stage Quadrupole Mass Spectrometer.

Supplemental Figure 1). The similar MSⁿ fragmentation patterns and the different RTs implied that the structure of feature-2 might be similar to that of DMED-DPA. Based on this, feature-2 was predicted to be a DMED-labeled candidate of neoDPA or *epi*-neoDPA.

To determine whether feature-2 was a downstream catabolite of neoPA, detached *Arabidopsis* siliques were incubated with H₂O, *d*₀-neoPA, or *d*₃-neoPA for 2 days (**Supplemental Figure 2**). The intensity of feature-2 detected from *d*₀-neoPA-treated siliques was significantly higher than that detected from H₂O-treated siliques (**Figure 2B**). From the *d*₃-neoPA-treated siliques rather than the H₂O-treated siliques, we detected a catabolite whose

parent ion m/z value was 3.0 units higher than that of feature-2, but its RT was identical to that of feature-2 (**Figure 2B**). These results suggested that the catabolite detected from the *d*₃-neoPA-treated siliques might be *d*₃-feature-2, which further indicated that feature-2 was a downstream catabolite of neoPA.

Previous studies have shown that PA can be reduced to DPA and *epi*-DPA by NaBH₄ (Hirai et al., 2003). Considering that the structure of neoPA is extremely similar to that of PA, we speculated that the reduced products of neoPA might be neoDPA and *epi*-neoDPA. To verify this speculation, we reduced neoPA with NaBH₄ and performed LC-MS analysis of the reduction products (**Supplemental Figure 3**). Two products

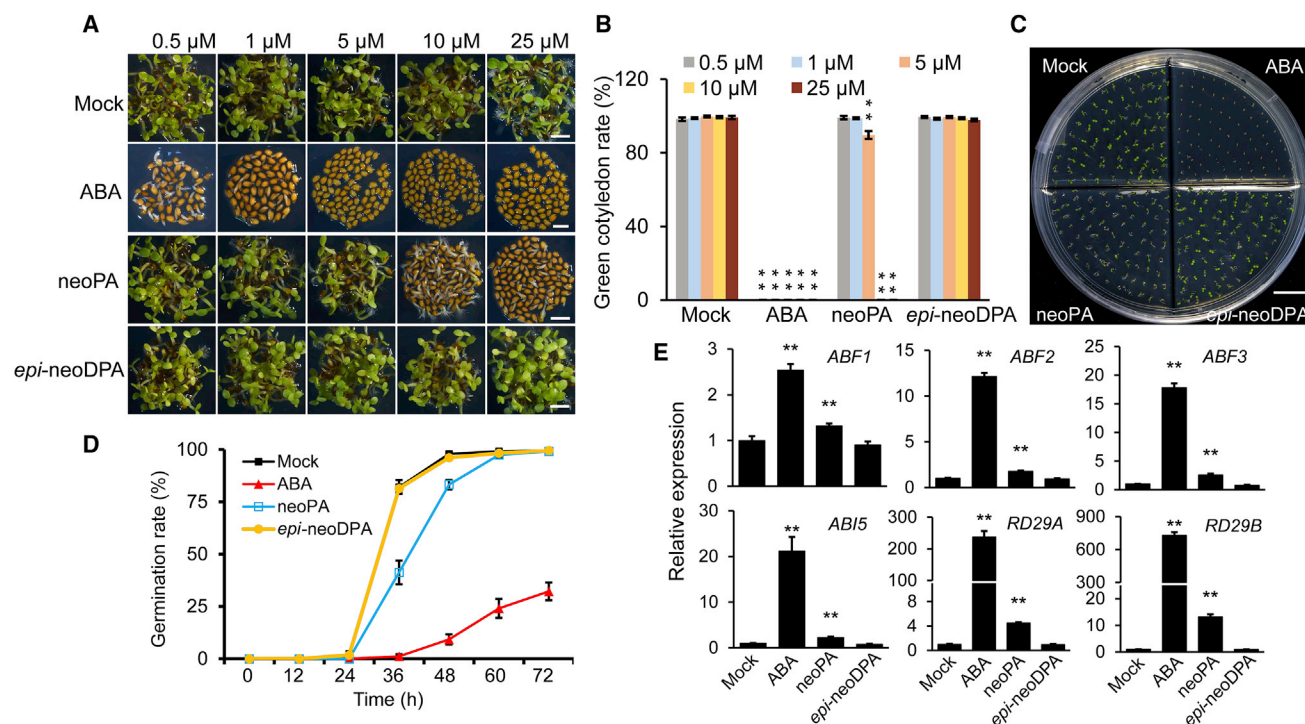


Figure 3. ABA-like activity of neoPA.

(A) Germination tests of *Arabidopsis* seeds on MS medium containing mock solution or various concentrations (0.5, 1, 5, 10, and 25 μ M) of ABA, neoPA, or *epi*-neoDPA. Photographs were taken at 60 h after stratification. Scale bars, 1 mm.

(B) Green cotyledon rates were quantified at 60 h after stratification. Data are means \pm SD of three independent experiments ($n \geq 100$ for each experiment; $**P < 0.01$, Student's *t*-test).

(C) Germination tests of *Arabidopsis* seeds on MS medium containing mock solution, 1 μ M ABA, 25 μ M neoPA, and 25 μ M *epi*-neoDPA. Photograph was taken at hour 72 after stratification. Scale bar, 1 cm.

(D) Germination rates at indicated time points. Data are expressed as means \pm SD of three replicates ($n \geq 100$ for each sample). Seeds with an emerging radicle were defined as germinated seeds.

(E) Relative expression levels of ABA-related genes in 7-day-old Col-0 seedlings treated with mock solution, 50 μ M ABA, neoPA, and *epi*-neoDPA for 3 h. *Actin2* expression was used as an internal control. Data are expressed as means \pm SD of three replicates. ($**P < 0.01$, Student's *t*-test).

were detected; their *m/z* value (281.2) was identical to that of neoDPA/*epi*-neoDPA, and their RTs were 9.15 min and 9.92 min, respectively, indicating that these two products might be neoDPA and *epi*-neoDPA.

With a very limited amount of neoPA, we failed to prepare enough reduction products for their accurate characterization. Therefore, their RT order was used to distinguish the neoDPA candidate from the *epi*-neoDPA candidate. The retention behavior of compounds with similar structures on the C18 column is closely related to their Log*P* values (Vrakas et al., 2005). Based on density functional theory (DFT), the Log*P* values of neoDPA, *epi*-neoDPA, DPA, and *epi*-DPA were estimated to be 0.585, 0.847, 0.514, and 0.607, respectively (Marenich et al., 2009) (Supplemental Table 5). The reduction products of PA with NaBH₄ were also prepared, and their RTs were determined to be 7.50 min and 9.26 min by LC-MS analysis (Supplemental Figure 3). The peak at 7.50 min was identified as DPA using authentic DPA, and the peak at 9.26 min was therefore assigned to *epi*-DPA. The above finding indicated that the RTs of the two compounds were positively correlated with the Log*P* values of DPA (0.514) and *epi*-DPA (0.607) (Supplemental Table 5). According to the calculated Log*P* values of neoDPA and *epi*-

neoDPA, the two peaks of the neoPA reduction products were further assigned. The peak at 9.15 min (Supplemental Figure 3) was assigned to the neoDPA candidate (Log*P* 0.585), and the peak at 9.92 min was assigned to the *epi*-neoDPA candidate (Log*P* 0.847) (Supplemental Figure 3 and Supplemental Table 5). Because the RT of the downstream catabolite detected from *Arabidopsis* siliques was identical to that of the *epi*-neoDPA candidate (Log*P* 0.847) (Supplemental Figure 3), our detected catabolite might be identified as the *epi*-neoDPA candidate.

In order to accurately identify the *epi*-neoDPA candidate, we chemically synthesized *epi*-neoDPA (Supplemental methods) and characterized it by 2D-NMR (Supplemental Figures 4–10). Consequently, the *epi*-neoDPA candidate detected from *Arabidopsis* siliques was identified as *epi*-neoDPA by comparing it with authentic *epi*-neoDPA (Figure 2C).

Biological activity of neoPA and *epi*-neoDPA

Previous studies have shown that PA in the ABA 8'-hydroxylation pathway has ABA-like hormonal activity, whereas DPA does not (Weng et al., 2016). In addition, neoPA and *epi*-neoDPA in the ABA 9'-hydroxylation pathway are isomers of PA and DPA, respectively, and their structures are extremely similar. Based

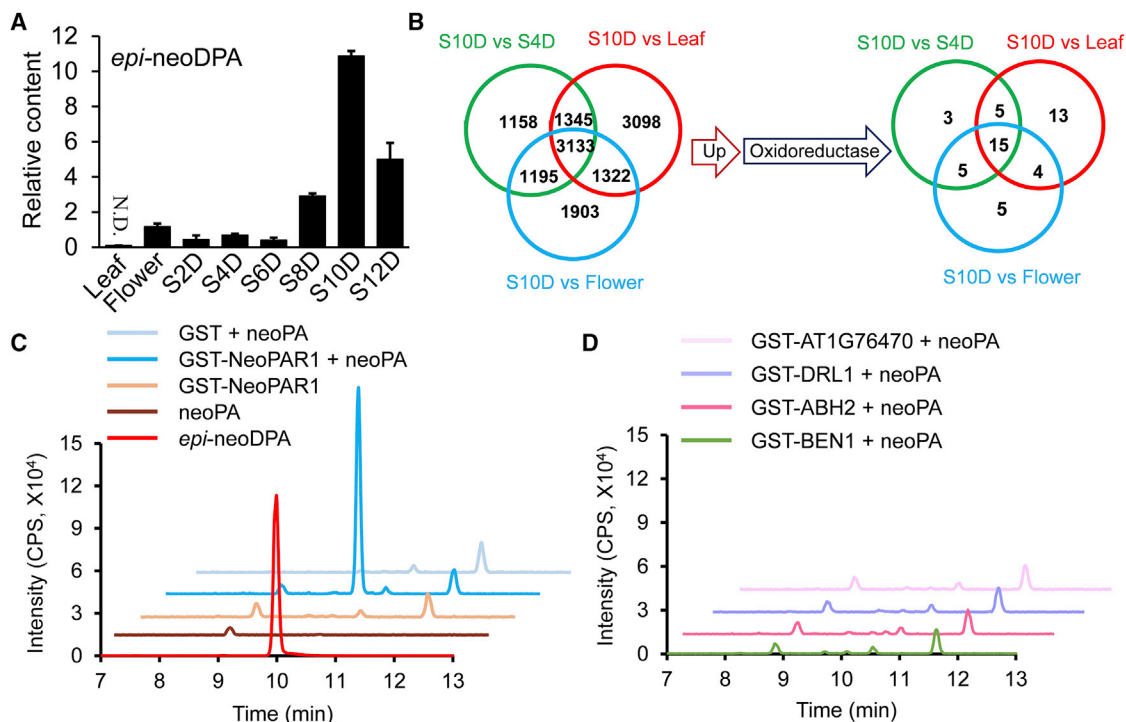


Figure 4. Identification of NeoPARs in *Arabidopsis*.

(A) Relative contents of *epi*-neoDPA in various *Arabidopsis* samples. Leaf, 6-week-old rosette leaf. S2D to S12D, siliques at day 2 to day 12 after pollination. N.D., not detected.

(B) Venn diagram of shared differentially expressed genes (DEGs, left) and upregulated oxidoreductase genes (right) in the comparisons of S10D versus S4D, S10D versus Leaf, and S10D versus Flower.

(C and D) MRM chromatograms of the products generated by the catalytic conversion of neoPA with the putative NeoPARs and controls at m/z 281.2 \rightarrow 171.2. Spectra were obtained on an AB SCIEX 4500 triple quadrupole mass spectrometer.

on these findings, we speculated that neoPA might possess ABA-like hormonal activity, whereas *epi*-neoDPA might not. Different concentrations of neoPA and *epi*-neoDPA were therefore applied to *Arabidopsis* seeds for a germination test. As shown in Figure 3A–3D, neoPA at low concentrations (0.5 μ M and 1 μ M) exhibited little inhibitory effect on seed germination, and 5 μ M neoPA showed a weak inhibitory effect on seed germination. By contrast, 10 μ M neoPA had a strong inhibitory effect, and 25 μ M neoPA had an even stronger inhibitory effect. However, *epi*-neoDPA in the tested concentration range (0.5–25 μ M) showed no inhibitory effect on seed germination (Figure 3A–3D). In conclusion, neoPA inhibits seed germination in a concentration-dependent manner, whereas *epi*-neoDPA exhibits no inhibitory effect on seed germination within the tested concentration range (0.5–25 μ M).

ABA-related genes such as *ABF1* (*ABA-responsive element binding factor 1*), *ABF2*, *ABF3*, *ABF4*, *ABI5* (*ABA-insensitive 5*), and the desiccation-responsive genes *RD29A* and *RD29B* play important roles in ABA signaling in *Arabidopsis* (Yamaguchi-Shinozaki and Shinozaki, 1994; Choi et al., 2000; Finkelstein and Lynch, 2000). To further characterize the hormonal activities of neoPA and *epi*-neoDPA, we analyzed the expression levels of these ABA-related genes in 5-day-old *Arabidopsis* seedlings treated with mock solution, ABA (50 μ M), neoPA (50 μ M), or *epi*-neoDPA (50 μ M) for 3 h. The ABA treatment caused a sharp increase in the expression of all the ABA-related

genes compared with the mock treatment (Figure 3E). The neoPA treatment also led to an increase in the expression of these ABA-related genes compared with the mock treatment, although the neoPA-induced increase was much lower than that induced by ABA. For example, the expression of *RD29B* was upregulated over 700-fold after ABA treatment but was upregulated only 13-fold after neoPA treatment. There were no significant differences in the expression levels of the ABA-related genes between the *epi*-neoDPA treatment and the mock treatment (Figure 3E). Taken together, our results indicate that neoPA still possesses partial ABA-like activity, whereas *epi*-neoDPA is a completely inactivated product of ABA.

Identification of neoPA reductase in *Arabidopsis*

To investigate the physiological function of the ABA 9'-hydroxylation pathway in plants, we first attempted to identify the neoPA reductase (NeoPAR) responsible for the conversion of neoPA into *epi*-neoDPA.

We hypothesized that the higher the NeoPAR gene expression level in plant tissues, the higher the *epi*-neoDPA content. Therefore, we identified the NeoPARs from the differentially expressed genes (DEGs) in plant tissues with different *epi*-neoDPA contents. Specifically, we first compared the *epi*-neoDPA, neoPA, and PA contents in *Arabidopsis thaliana* rosette leaves, flowers, and siliques at different developmental stages, including siliques 2 days after

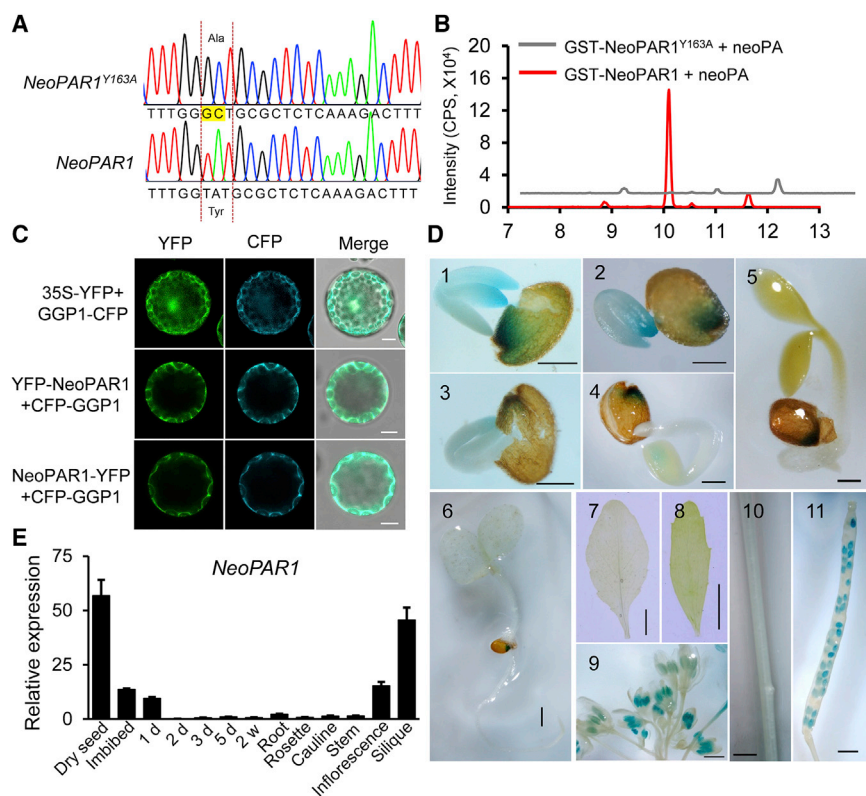


Figure 5. Expression properties of NeoPAR1.

(A) Site-directed mutation at NeoPAR1^{Y163A} by DNA sequencing.

(B) MRM chromatograms of the products generated from the catalytic conversion of neoPA by GST-NeoPAR1 and GST-NeoPAR1^{Y163A} at *m/z* 281.2 → 171.2.

(C) Cytosolic localization of YFP-NeoPAR1 and NeoPAR1-YFP in protoplasts of Arabidopsis. GGP1-CFP, cytosol marker. 35S-YFP, empty vector control. Scale bars, 10 μm.

(D) Expression of NeoPAR1pro-GUS in seeds, early germinated seedlings, anthers, and siliques. 1, dry seed; 2, seeds imbibed for 48 h; 3 to 6, germinated seedlings at day 1, day 2, day 3, and day 5; scale bars represent 0.5 mm (for 1–6); 7, rosette leaf; 8, cauline leaf; scale bars represent 0.5 cm (for 7–8); 9, inflorescence; 10, stem; 11, siliques; scale bars represent 1 mm (for 9–11).

(E) Relative expression of NeoPAR1 measured by RT-qPCR. Imbibed, seeds imbibed for 48 h; 1–5 d, germinated seedlings at day 1, day 2, day 3, and day 5; Root, rosette leaf, cauline leaf, and stem were sampled from 6-week-old Arabidopsis plants. Data are expressed as means ± SD of three replicates.

pollination (S2D), S4D, S6D, S8D, S10D, and S12D (Supplemental Figure 11 and Figure 4A). The results showed that S10D exhibited the highest amount of *epi*-neoDPA, whereas rosette leaves contained no *epi*-neoDPA (Figure 4A). The results also showed that the changes in neoPA and *epi*-neoDPA content were consistent in these tissues (Supplemental Figure 11 and Figure 4A). Next, we selected four tissues with large differences in *epi*-neoDPA contents (rosette leaves, flowers, S4D, and S10D) for transcriptome analysis. A total of 7553 DEGs were identified in the comparison of S10D versus flowers, 8898 DEGs in S10D versus leaves, and 6832 DEGs in S10D versus S4D (Figure 4B). A Venn diagram showed 3133 shared DEGs in the above-mentioned three comparisons (Figure 4B), from which we selected 15 significantly upregulated potential NeoPARs encoding oxidoreductases (GO:0016491) (supplementary Table 6). We further examined the expression levels of these 15 genes in the four tissues by RT-qPCR and found that all their expression levels were significantly higher in S10D than in the other three tissues. The RT-qPCR results were consistent with the transcriptomic data, which confirmed the reliability of the transcriptomic results (sSupplemental Figure 12). Four out of the 15 genes were predicted to belong to the NAD(P)-binding Rossmann-fold superfamily. Because the two PARs (ABH2 and CRL1) have also been reported to belong to this superfamily (Weng et al., 2016; Yin et al., 2022), we cloned and expressed these four genes and a predicted reductase gene (*Dihydroflavonol 4-reductase-like 1*, *DRL1*) in a bacterial system (Supplemental Table 6). The reduction tests of the purified recombinant proteins revealed that only the protein encoded by *AT1G09510* exhibited neoPA reduction activity (Figure 4C and 4D), and this protein was therefore named NeoPAR1 (neoPA reduc-

tase 1). In addition, the PA reduction tests of the proteins suggested that NeoPAR1 also showed a very weak PA reduction activity, which was about 0.3% that of ABH2 (Supplemental Figure 13A). The neoPA reduction test of CRL1 showed that CRL1 could not convert neoPA into *epi*-neoDPA (Supplemental Figure 13B).

NeoPAR1 expression in cells and tissues

Our previous study revealed that PARs (CRL1 and ABH2) contain a conserved YXXXK motif whose tyrosine (Tyr, Y) residue is essential for catalytic activity (Yin et al., 2022). In this study, protein sequence alignment analysis indicated that NeoPAR1 also contains a conserved YXXXK motif with a Y163 residue (Supplemental Figure 14). When the Y163 residue was mutated into alanine (A), the neoPA reductase activity of NeoPAR1 was abolished, suggesting that Y163 in the YXXXK motif is crucial for the neoPA reductase activity of NeoPAR1 (Figure 5A and 5B).

To better understand the possible *in vivo* function of NeoPAR1, we analyzed the expression properties of NeoPAR1 both qualitatively and quantitatively. To assess the cellular localization of NeoPAR1, YFP-fused NeoPAR1 and the cytosolic marker CFP-fused γ -glutamyl peptidase GGP1 (Geu-Flores et al., 2011) were transiently expressed in Arabidopsis protoplasts under the CaMV 35S constitutive promoter, and the results showed that YFP-fused NeoPAR1 was mainly localized in the cytosol (Figure 5C). Next, we assessed the temporal and spatial expression patterns of NeoPAR1 in transgenic Arabidopsis plants expressing a β -glucuronidase (GUS) reporter driven by the NeoPAR1 promoter. After GUS staining, dry seeds, imbibed seeds, germinated seeds, young seedlings, and adult plants were readily observed. GUS staining was primarily observed in

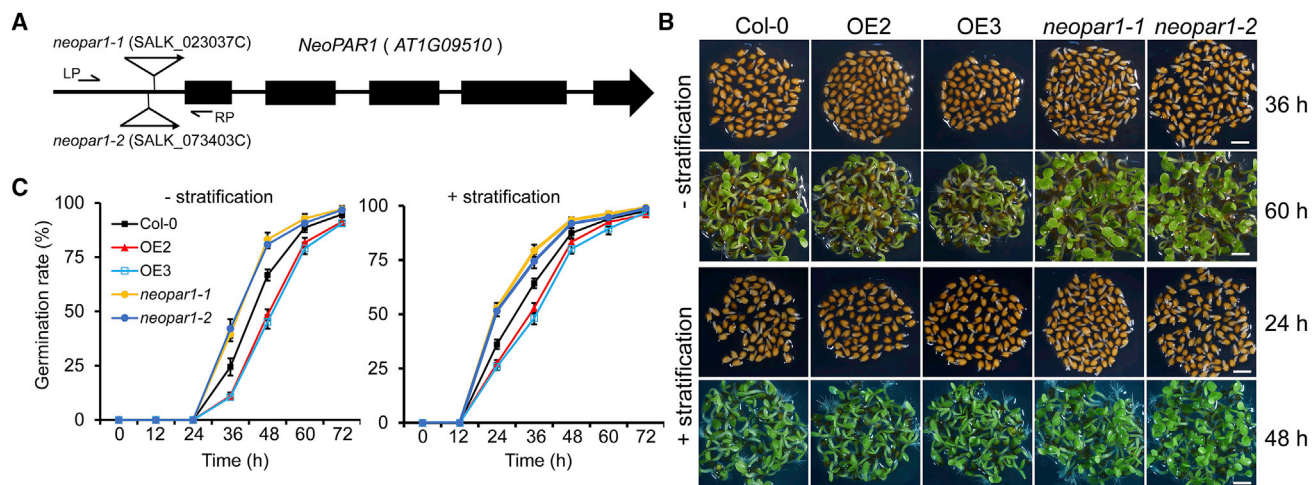


Figure 6. Phenotypic characterization of *NeoPAR1* transgenic lines during seed germination.

(A) Genomic map of the *NeoPAR1* locus. The triangles indicate the positions of T-DNA insertions in *neopar1-1* and *neopar1-2*. LP, left primer; RP, right primer.

(B) Germination tests of *Arabidopsis* seeds on MS plates without (upper panel) and with (lower panel) 2-day stratification treatment. Scale bars, 1 mm.

(C) Germination rates at the indicated time points in Col-0, OE2, OE3, *neopar1-1*, and *neopar1-2* grown on MS without (left panel) and with (right panel) 2-day stratification treatment. Data were generated using four seed lots generated from bulks of independent plants that had been produced at two different times, and similar results were obtained from these seed lots. Data are expressed as means \pm SD of three replicates ($n \geq 100$ for each sample).

cotyledons of dry seeds, chalazal seed coats, young anthers, and siliques. During germination, the GUS signal intensity diminished with seedling morphogenesis, and it was hardly visible in 3-day-old seedlings (Figure 5D). RT-qPCR analysis of *NeoPAR1* from various *Arabidopsis* tissues (dry seeds, imbibed seeds, germinated seedlings, 2-week-old seedlings, 6-week-old plants, and siliques) indicated that *NeoPAR1* was predominantly expressed in dry seeds and siliques, consistent with the GUS staining results (Figure 5E). These results suggest that *NeoPAR1* may play an important role in seed germination, stamen development, and seed ripening in *Arabidopsis*.

Regulation of seed germination by *NeoPAR1*

To investigate the roles of *NeoPAR1* in seed germination in *Arabidopsis*, we characterized the two homozygous T-DNA insertion mutants *neopar1-1* (SALK_023037C) and *neopar1-2* (SALK_073403C, Supplemental Figure 15A). Both *neopar1-1* and *neopar1-2* still showed weak expression of *NeoPAR1* due to the two T-DNA insertions at the 5'-UTR (Figure 6A). The RT-qPCR results indicated that the expression levels of *NeoPAR1* in the *neopar1-1* and *neopar1-2* mutants were about 7.5% and 17.6% of that in the wild type (Col-0), respectively (Supplemental Figure 15B). We also constructed transgenic lines overexpressing *NeoPAR1* (OE), and two lines (OE2 and OE3) with moderately elevated *NeoPAR1* expression levels were used for further analysis (Supplemental Figure 15B).

Considering the fact that *NeoPAR1* is involved in the downstream catabolism of ABA and shows relatively high expression in dry seeds, we speculated that changes in *NeoPAR1* expression would influence seed germination in *Arabidopsis*. We therefore compared the seed germination of the *NeoPAR1* OEs, *neopar1-1*, and *neopar1-2* with that of Col-0 plants. OE2 and OE3 germinated much more slowly than Col-0, with or without a 2-day stratification treatment, whereas *neopar1-1* and *neopar1-2* germinated signifi-

cantly faster than Col-0 (Figure 6B and 6C). Next, we constructed *neopar1* knockout mutants using the CRISPR-Cas9 genome editing system. Two Cas9-free mutants (*cas9-1* and *cas9-3*) with different types of base pair deletions in the fourth exon of *NeoPAR1* were identified by fluorescence screening, genomic DNA PCR, and sequencing (Supplemental Figure 16A–16D). Seed germination analysis indicated that *cas9-1* and *cas9-3* germinated much faster than Col-0, similar to *neopar1-1* and *neopar1-2* (Supplemental Figure 16E and 16F). We also compared the germination rates of non-sterilized seeds of Col-0, OE2, OE3, *neopar1-1*, *neopar1-2*, and *cas9-1* grown directly on water at 23°C and 32°C, as temperature may change the seed germination rate. The results also showed that OE2 and OE3 germinated faster than Col-0 and *neopar1-1*, *neopar1-2*, and *cas9-1* germinated more slowly than Col-0 at both 23°C and 32°C (Supplemental Figure 17). Interestingly, we noticed that the loss-of-function mutant *abh2-1* also germinated more slowly than Col-0 (Supplemental Figure 18). These results suggest that *NeoPAR1* slows seed germination, whereas *ABH2* accelerates it. Taken together, our results suggest that *NeoPAR1* may play an important role in seed germination.

Regulation of ABA metabolism by *NeoPAR1*

To further explore the biochemical roles of *NeoPAR1* in ABA metabolism *in vivo*, we measured the contents of neoPA, *epi*-neoDPA, and ABA in freeze-dried seeds of Col-0, OE2, OE3, *neopar1-1*, *neopar1-2*, and *cas9-1* using LC-MS. The results showed that OE2 and OE3 accumulated high levels of *epi*-neoDPA, whereas *neopar1-1*, *neopar1-2*, and *cas9-1* contained less *epi*-neoDPA than Col-0, consistent with the finding that *NeoPAR1* converted neoPA into *epi*-neoDPA (Figure 7A). The neoPA content was below the limit of quantification in all three lines (Figure 7A). Notably, the ABA content was significantly lower in *neopar1-1*, *neopar1-2*, and *cas9-1* than in Col-0, but it was much higher in OE2 and OE3 than in Col-0 (Figure 7A). We

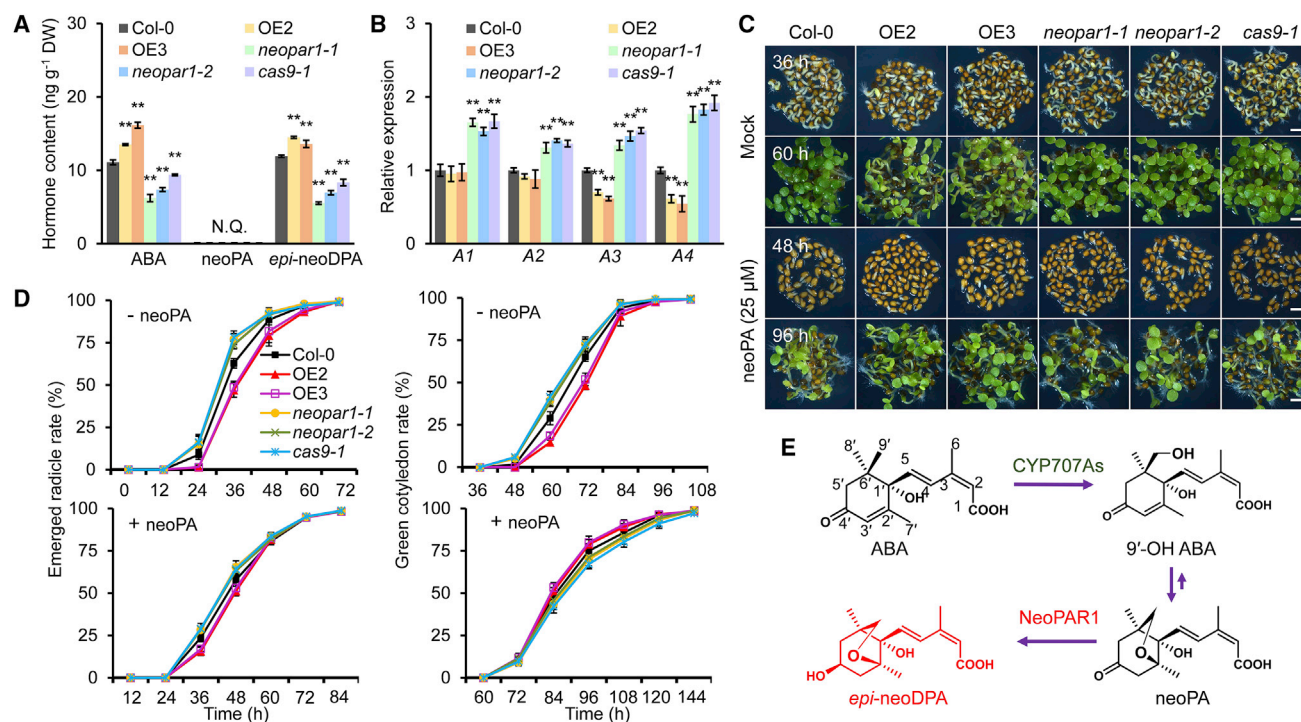


Figure 7. Conversion of neoPA into *epi*-neoDPA by NeoPAR1 in *Arabidopsis* plants.

(A) Quantitation of ABA, neoPA, and *epi*-neoDPA in freeze-dried seeds. Data are expressed as means \pm SD of three replicates (** $P < 0.01$, Student's *t*-test). N.Q., not quantified.

(B) Relative expression of the ABA catabolic genes *CYP707A1–A4* in the dry seeds of Col-0, OE2, OE3, *neopar1-1*, *neopar1-2*, and *cas9-1*. A1–A4, *CYP707A1–A4*. Gene expression was normalized based on the expression level of Col-0 as a reference. Data are expressed as means \pm SD of three replicates (**, $P < 0.01$, Student's *t*-test).

(C) Germination tests of *Arabidopsis* seeds on MS plates without (upper panel) and with (lower panel) the addition of 25 μ M neoPA. Scale bar, 1 mm.

(D) Emerged radicle and green cotyledon rates were quantified at the indicated time points in Col-0, OE2, OE3, *neopar1-1*, *neopar1-2*, and *cas9-1* grown on MS without and with the addition of 25 μ M neoPA. Data were generated using four seed lots generated from bulks of independent plants that had been produced at two different times, and similar results were obtained from these seed lots. Data are expressed as means \pm SD of three replicates ($n \geq 100$ for each sample).

(E) Working model of the 9'-hydroxylation catabolism pathway of ABA.

next investigated the expression of the *CYP707As* involved in ABA catabolism and found that the four genes *CYP707A1–A4* were downregulated in OE2 and OE3 compared with Col-0, but they were upregulated in *neopar1-1*, *neopar1-2*, and *cas9-1* (Figure 7B). To investigate the effect of neoPA on NeoPAR1, we compared the seed germination of OE2, OE3, *neopar1-1*, *neopar1-2*, and *cas9-1* with that of Col-0 after the application of 25 μ M neoPA. The results showed that neoPA inhibited seed germination in all three lines, but the inhibition effect of neoPA was much weaker on OE2 and OE3 than on Col-0 (Figure 7C and 7D). Overall, we identified a new neoPA reductase involved in ABA catabolism, NeoPAR1 (Figure 7E); it not only directly catalyzes neoPA but also modulates ABA homeostasis in *Arabidopsis*.

DISCUSSION

We conducted a comprehensive and in-depth investigation of the ABA 9'-hydroxylation pathway in *Arabidopsis thaliana* and found that neoPA was catabolized into *epi*-neoDPA by NeoPAR1. In addition, neoPA rather than *epi*-neoDPA exhibited an inhibitory effect on seed germination and regulated ABA-related gene

expression. NeoPAR1 plays important roles in *Arabidopsis* seed germination. This discovery extends our knowledge about the 9'-hydroxylation catabolism pathway of ABA.

Different enzymes catalyzed catabolism of neoPA and PA in *Arabidopsis*

neoPA and PA in the ABA 9'- and 8'-hydroxylation pathways, respectively, share extremely high structural similarity and have ABA-like activity in seed germination. In addition, 9'- and 8'-hydroxylation are catalyzed by the same monooxygenases, *CYP707As*. ABH2 and CRL1 have previously been reported to convert PA into DPA in the 8'-hydroxylation pathway (Weng et al., 2016; Yin et al., 2022). However, we found that ABH2 or CRL1 was not able to catalyze neoPA to yield *epi*-neoDPA *in vitro* (Figure 4D). In this study, we identified NeoPAR1 with neoPA reductase activity in *Arabidopsis* by analysis of *epi*-neoDPA content in combination with transcriptome analysis (Figure 4A–4C). The difference in catabolism between neoPA and PA suggests that they may be under the control of different regulatory mechanisms in response to different physiological processes. Nevertheless, we found that NeoPAR1, ABH2, and

CRL1 contained a conserved YXXXK motif and that the Tyr residues were critical to the reduction activity (Supplemental Figure 14 and Figure 5A and B), suggesting that the catalytic mechanisms of NeoPAR1 and PARs may be similar. In addition, neoPA, similar to PA, possesses partial ABA-like activity (Figure 3). PA has been reported to selectively activate a subset of ABA receptor family members and alter some ABA-responsive genes, as well as a small but unique PA-responsive gene set of its own (Weng et al., 2016). We therefore speculate that neoPA may also be able to activate a subset of ABA receptors and trigger its own responsive genes. However, this speculation needs to be verified in future research.

NeoPAR1 affects seed germination by regulating ABA levels in *Arabidopsis*

Previous studies have shown that loss of the PAR ABH2 in the 8'-hydroxylation pathway leads to elevated ABA sensitivity during seed germination and PA accumulation in *Arabidopsis* without affecting ABA levels (Weng et al., 2016). Our results suggest that the ABH2 null mutant *abh2-1* showed delayed seed germination without ABA application (Supplemental Figure 18), which may be due to inhibition of seed germination by the accumulated PA in an ABA-like manner. Our recent study also showed that the loss of CRL1, another PAR, also leads to slower germination and reduced PA accumulation without affecting ABA levels (Yin et al., 2022). The 9'-hydroxylation pathway is widespread in various plants and may thus have some specific physiological functions (Zhou et al., 2004). In this study, we found that seed germination of *neopar1-1* was accelerated (Figure 6B and 6C) and that seed ABA content was lower in *neopar1-1* than in Col-0 (Figure 7A). In addition, the expression levels of CYP707As in the seeds were higher in *neopar1-1* than in Col-0 (Figure 7B). It is thought-provoking that NeoPAR1 and PARs (ABH2 and CRL1) have opposite effects on seed germination. Owing to the high similarity of the ABA 8'- and 9'-hydroxylation pathways, we might easily suppose that the phenotypes of NeoPAR1 mutants would resemble those of PAR mutants. However, 9'-hydroxylation is considered only a side reaction of 8'-hydroxylation, as the catabolite levels in the 9'-hydroxylation pathway are usually very low (Chen et al., 2020). PARs such as ABH2 and CRL1 cannot catalyze neoPA, whereas NeoPAR1 shows weak PA reductase activity, suggesting that NeoPAR1 may have a different function from PARs. Indeed, our results showed that the absence of NeoPAR1 causes a significant reduction in ABA levels (Figure 7A), which is not consistent with the PAR knockout mutants (Weng et al., 2016; Yin et al., 2022). Hence, the phenotypes of NeoPAR1 mutants may be caused largely by abnormal ABA levels because ABA has much stronger biological activity than neoPA (Figure 3). In addition, the weak PA activity of NeoPAR1 also reveals that NeoPAR1 may play multiple roles in the ABA metabolism pathway, whereas ABH2 and CRL1 may have more specific and efficient catalytic activity than NeoPAR1, which contributes to keeping the main ABA catabolite PA at a relatively low level. The opposite phenotypes of NeoPAR1 and PARs also indicate that 9'-hydroxylation may not be a side reaction of 8'-hydroxylation. The accumulated *epi*-neoDPA seems to exert feedback inhibition on ABA catabolism in NeoPAR1 OE2, whereas the reduced *epi*-neoDPA may accelerate ABA catabolism in *neopar1-1* (Figure 7A and 7B). Therefore, the NeoPAR1-mediated 9'-hydroxylation pathway may have an

important modulation role in plant ABA homeostasis. However, the specific modulation mechanisms remain unclear. Further studies of the comprehensive metabolic network (including biosynthesis, catabolism, and transport) and signaling network of ABA will contribute to elucidating the modulation mechanism of the ABA 9'-hydroxylation pathway.

METHODS

Plant materials and growth conditions

All *Arabidopsis* plants were of the Col-0 ecotype. The *neopar1-1* (SALK_023037C) and *neopar1-2* (SALK_073403C) mutants were obtained from the ABRC (<https://abrc.osu.edu>). Homozygous mutant plants were identified according to a reported method (Alonso et al., 2003). All transgenic plants were generated via the floral dip method (Clough and Bent, 1998). The OE lines were produced by transforming the pBA002-NeoPAR1 vector into plants in the Col-0 background. Homozygous plants in the T3 generation were identified and used for subsequent analysis. NeoPAR1 was knocked out by the CRISPR-Cas9 system to obtain mutants, and Cas9-free mutants were isolated according to a reported protocol (Gao et al., 2016b). In brief, an sgRNA from the fourth exon was fused into the pHDE-35SCas9-mCherry vector to target *NeoPAR1*. Because T1 transgenic seeds containing the Cas9 protein also contained the mCherry protein, they could be isolated under a dissecting fluorescence microscope (SMZ1500, Nikon, Japan). Non-fluorescent Cas9-free T2 seeds were also isolated through a fluorescence screen and verified by genomic PCR and sequencing. Plants were grown in a growth room under a 16-h light/8-h dark cycle at 23°C. Seeds with the same storage periods were used for the seed germination assay. Seeds were surface sterilized with 1% sodium hypochlorite and sown on Murashige and Skoog (MS) (PhytoTechnology, USA) plates containing 0.8% (w/v) agar. After a 2-day stratification at 4°C in the dark, the seeds were transferred to a growth chamber. Seeds with an emerging radicle were defined as germinated seeds (Zhao et al., 2015). Four seed lots generated from bulks of independent plants that had been produced at two different times were used for germination, and similar results were obtained from these seed lots. For each germination test, at least 100 seeds were used. All germination experiments were performed in at least triplicate. The data were analyzed using Microsoft Excel and expressed as the mean \pm standard deviation (SD). Significant differences analyzed using Student's *t*-tests are presented at **P* < 0.05 and ***P* < 0.01.

Siliques were treated with *d*₀-neoPA (2 mg/L in H₂O) and *d*₃-neoPA (2 mg/L in H₂O) for two days in a growth room under a 16-h light/8-h dark cycle at 23°C, and siliques in the control group were treated with H₂O. A standard solution of *d*₃-neoPA (2 mg/L in H₂O) was incubated under the same conditions to investigate whether there was spontaneous transformation *in vitro*.

Discovery of downstream catabolites of neoPA

One hundred milligrams of *Arabidopsis* siliques were used to discover downstream catabolites of neoPA. The sample preparation procedure consisted of solvent extraction, solid phase extraction, and chemical labeling (with the details of sample pre-treatment and chemical labeling presented in supplemental information). Equal amounts of DMED-labeled plant samples and *d*₄-DMED-labeled plant samples were mixed and subjected to LC-MS analysis to screen downstream catabolites of neoPA (instrumentation and analytical conditions shown in supplemental information). One gram of *Arabidopsis* siliques was used for MSⁿ analysis because the intensity of feature-2 was too low to obtain its MS²-MS⁴ spectra when 100 mg siliques were used.

Chemical synthesis

The schemes for reduction of PA and neoPA are shown in Supplemental Figure 3A. A 0.2- μ g quantity of PA/neoPA was dissolved in 100 μ L MeOH in a 1.5-mL centrifuge tube. The solution was cooled to 0°C, and 0.6 mg NaBH₄ was added. The reaction was performed at 60°C for

12 h. Afterwards, 10 μ L of 0.12 M HCl was added, and reaction products were extracted using 1 mL ethyl acetate.

The schemes for synthesis of neoPA and *epi*-neoDPA are shown in [Supplemental Scheme 2](#), and detailed methods are shown in [supplemental information](#).

Computational methods

Conformational search, geometry optimization, frequency analysis, and single-point-energy calculation were performed to calculate LogP values of DPA, *epi*-DPA, neoDPA, and *epi*-neoDPA using Molclus-1.9.4 (Lu, 2020), ORCA-4.2.1 (Neese, 2012, 2018), and Gaussian 09 (Frisch et al., 2013). In brief, the input geometries were constructed by GaussView. The initial conformers were batch generated by the “gentor” module in the Molclus program. Single-point energies of batch conformers were calculated using MOPAC by the semi-empirical method PM7, and batch conformers were clustered based on an energy threshold of 0.5 kcal/mol and a geometry threshold of 0.25 Å via the “isostat” module in Molclus. The top 200 clusters with the lowest energy were preliminarily optimized using MOPAC by the semi-empirical method PM7 and clustered again based on an energy threshold of 0.5 kcal/mol and a geometry threshold of 0.25 Å. The obtained top 10 clusters were re-optimized using the ORCA program package at the advanced theory level of B3LYP-D3(BJ) 6-311G* and re-clustered. The conformers with lowest energy were subjected to geometry optimization and frequency analysis at the B3LYP/6-311+G* level to obtain the minimum-energy structures (Cartesian coordinates shown in [Supplemental Tables 1–4](#)) with zero imaginary frequencies in gas phase using the Gaussian 09 program. Single-point energies were calculated by the DFT method at the M052-2X/6-31G* level with the SMD continuum solvent model (Marenich et al., 2009), and single-point energies of the conformers in *n*-octanol were defined as E_{oct} and in water as E_{w} . Finally, LogP was calculated according to the formula $\text{LogP} = -(E_{\text{oct}} - E_{\text{w}})/2.303 \times R \times T$, and the results are listed in [Supplemental Table 5](#).

RNA-Seq and transcriptome analysis

Mature leaves (150 mg) of 6-week-old *Arabidopsis* WT (Col-0), flowers in full bloom, and 4- and 10-day-old siliques were used for RNA-seq. RNA extraction, multiplex RNA library construction, and Illumina sequencing were carried out by PersonalGene (Nanjing, China). Approximately 42 million reads of 300-base-pair (bp) paired-end sequences were generated for each sample. Raw reads were mapped onto the *Arabidopsis* gene models using HISAT2 (Kim et al., 2019). The reads corresponding to each gene were counted using featureCounts in the Subread package (Liao et al., 2014). Differential gene expression was evaluated using DESeq2 (Love et al., 2014). Oxidoreductase genes were screened based on GO (Gene Ontology) analysis (<http://amigo.geneontology.org/amigo/landing>).

RT-qPCR assays

Total RNA was extracted using the RNAprep Pure Plant Plus Kit (TIANGEN, China) from 50 mg of sample (dry seeds, imbibed seeds, germinated seedlings, leaves, flowers, and siliques at the indicated times) for RT-qPCR quantification of gene expression. RNA samples were reverse-transcribed with the ABScript II cDNA First-Strand Synthesis Kit (ABclonal, China). The cDNA was amplified using TransStart Top Green qPCR SuperMix (TransGen, China) on a CFX Connect Real-Time PCR Detection System (Bio-Rad, USA). The expression level of *ACTIN2* (*At3g18780*) was used as an internal control. The primer sequences used for the RT-qPCR experiments are listed in [Supplemental Table 7](#).

Plasmid construction

For expressing recombinant protein, the CDSs of the five candidate genes, *AT1G76470* (978 bp), *AT1G09510* (*NeoPAR1*, 969 bp), *AT4G35420* (*DRL1*, 981 bp), *AT4G27250* (*ABH2*, 1065 bp), and *AT2G45400* (*BEN1*, 1095 bp), were amplified from siliques of *Arabidopsis* using the reverse transcription polymerase chain reaction (RT-PCR) and cloned into the pGEX-4TI vector (GE Healthcare, USA). *NeoPAR1* site-directed mutagenesis was performed

by overlap extension PCR with a pair of overlapping PCR primers (Edelheit et al., 2009). To generate the *NeoPAR1*-overexpressing transgenic lines (OE), the pBA002-*NeoPAR1* vector was constructed by inserting a cassette containing the CaMV 35S promoter (35S) and the full-length *NeoPAR1* CDS into the binary vector pBA002. The promoter sequence (2.0 kb upstream of the start codon ATG) was amplified from the genomic DNA of Col-0 for a histochemical GUS assay. The amplified PCR fragment was then inserted into the binary vector pBI101. For the transient expression assay, the p35S-YFP-*NeoPAR1* vector was constructed as described previously (Yin et al., 2019). Information on the primers used for vector construction and transgenic line generation is presented in [Supplemental Table 8](#).

Recombinant protein production and *in vitro* enzyme assay

All the recombinant proteins were expressed in *Escherichia coli* (*E. coli*, BL21, Condon plus) harboring the corresponding plasmid. Protein expression was induced with 0.5 mM IPTG (isopropyl- β -D-thiogalactopyranoside) for 16 h at 18°C. Bacterial cells were harvested by centrifugation (10,000 *g*, 10 min), then resuspended in PBS buffer (pH 7.2) containing 1 mM PMSF, and finally lysed by sonication. The expressed protein was isolated from the *E. coli* lysate by affinity chromatography with glutathione sepharose beads (GE Healthcare, USA) and eluted with elution buffer (50 mM Tris-HCl, 20 mM reduced glutathione, pH 8.0). The purified GST (glutathione S-transferase) from the *E. coli*-expressed empty vector pGEX-4TI was used as the control. The enzymatic assays were performed in buffer (100 mM Tris-HCl, pH 7.0) in the presence of 500 μ M NADPH and 50 μ M neoPA. Recombinant protein (5 μ g) was added to the enzymatic assay system (50 μ l) to initiate the reaction. The reaction lasted for 12 h at 22°C and was terminated by addition of glacial acetic acid. The reaction mixture was extracted with ethyl acetate. The extract was dried in nitrogen and redissolved in 10% (v/v) ACN/H₂O, and the final reaction product *epi*-neoDPA was quantified by LC-MS.

Histochemical GUS assay and transient expression assays

Histochemical analysis of GUS expression in *NeoPAR1* pro-GUS plants was performed as described previously (Jefferson et al., 1987). More than 50 independent T1 GUS lines were isolated, and 10 of them (T3 generation) were used for further analysis. Among the 10 GUS lines, eight lines exhibited the same expression pattern. Photographs were captured with a stereomicroscope (Nikon SMZ1500, Japan) or a Canon EOS 70D digital camera (Canon, Japan). Mesophyll protoplasts were isolated and transformed following a previously described protocol (Yoo et al., 2007). Plasmids p35S-YFP and p35S-YFP-*NeoPAR1* were transformed into mesophyll protoplasts. Specifically, approximately 10 μ g plasmid DNA, 100 μ L protoplast suspension, and 110 μ L 40% polyethylene glycol 4000 solution containing 0.2 M mannitol and 100 mM CaCl₂ were gently mixed for each transformation. The mixture was incubated at room temperature for 15 min, and 440 μ L W5 solution (containing 2 mM MES, pH 5.7, 154 mM NaCl, 5 mM KCl, and 125 mM CaCl₂) was added to stop the transformation. The protoplasts were collected by centrifugation, resuspended in W5 solution, and incubated at 23°C in the dark. All the images were captured with a confocal laser scanning microscope (TCS SP8, Leica, Germany).

LC-MS quantification of ABA-related catabolites

ABA and its catabolites were extracted from *Arabidopsis*, and the extracts were pretreated according to our previously reported method (Bai et al., 2018) and analyzed on an HPLC-MS system (instrumentation and analytical conditions shown in [supplemental information](#)).

ACCESSION NUMBERS

A reporting summary for this article is available as a [supplemental information](#) file. All data supporting the findings of this study are available from the corresponding authors upon reasonable request.

SUPPLEMENTAL INFORMATION

Supplemental information can be found online at [Plant Communications Online](#).

FUNDING

This work is supported by the National Key R&D Program of China (2018YFA0900400) and the National Natural Science Foundation of China (21635006, 31670373, 21721005).

AUTHOR CONTRIBUTIONS

Y.L.B., X.M.Y., and Y.Q.F. designed the experiments and wrote the paper. Y.L.B., X.M.Y., and C.F.X. conducted the experiments and analyzed the data. X.J.Z. and Y.W. provided suggestions. T.T.Y., B.D.C., Z.W.W., and Y.Q.F. revised the paper. All authors discussed the results and edited the manuscript.

ACKNOWLEDGMENTS

We thank Dr. Yunde Zhao (University of California, San Diego, USA) for providing the CRISPR-Cas9 plasmid. Great gratitude goes to linguistics Prof. Ping Liu from Huazhong Agricultural University, Wuhan, China for English editing and language polishing. No conflict of interest declared.

Received: January 15, 2022

Revised: May 6, 2022

Accepted: May 12, 2022

Published: May 17, 2022

REFERENCES

- Alonso, J.M., Stepanova, A.N., Leisse, T.J., Kim, C.J., Chen, H., Shinn, P., Stevenson, D.K., Zimmerman, J., Barajas, P., Cheuk, R., et al. (2003). Genome-wide insertional mutagenesis of *Arabidopsis thaliana*. *Science* **301**:653–657. <https://doi.org/10.1126/science.1086391>.
- Bai, Y.-L., Cai, B.-D., Luo, X.-T., Ye, T.-T., and Feng, Y.-Q. (2018). Simultaneous determination of abscisic acid and its catabolites by hydrophilic solid-phase extraction combined with ultra high performance liquid chromatography–tandem mass spectrometry. *J. Agr. Food Chem.* **66**:10906–10912. <https://doi.org/10.1021/acs.jafc.8b03820>.
- Cai, W.-J., Zeng, C., Zhang, X.-Y., Ye, T., and Feng, Y.-Q. (2021). A structure-guided screening strategy for the discovery and identification of potential gibberellins from plant samples using liquid chromatography-mass spectrometry assisted by chemical isotope labeling. *Anal. Chim. Acta* **1163**:338505. <https://doi.org/10.1016/j.aca.2021.338505>.
- Chen, K., Li, G.-J., Bressan, R.A., Song, C.-P., Zhu, J.-K., and Zhao, Y. (2020). Abscisic acid dynamics, signaling and functions in plants. *J. Integr. Plant Biol.* **62**:25–54. <https://doi.org/10.1111/jipb.12899>.
- Choi, H.-I., Hong, J.-H., Ha, J.-O., Kang, J.-Y., and Kim, S.Y. (2000). ABFs, a family of ABA-responsive element binding factors. *J. Biol. Chem.* **275**:1723–1730. <https://doi.org/10.1074/jbc.275.3.1723>.
- Clough, S.J., and Bent, A.F. (1998). Floral dip: a simplified method for *Agrobacterium*-mediated transformation of *Arabidopsis thaliana*. *Plant J.* **16**:735–743. <https://doi.org/10.1046/j.1365-313x.1998.00343.x>.
- Cutler, S.R., Rodriguez, P.L., Finkelstein, R.R., and Abrams, S.R. (2010). Abscisic acid: emergence of a core signaling network. *Annu. Rev. Plant Biol.* **61**:651–679. <https://doi.org/10.1146/annurev-arplant-042809-112122>.
- Dong, T., Park, Y., and Hwang, I. (2015). Abscisic acid: biosynthesis, inactivation, homeostasis and signalling. *Essays Biochem.* **58**:29–48. <https://doi.org/10.1042/bse0580029>.
- Edelheit, O., Hanukoglu, A., and Hanukoglu, I. (2009). Simple and efficient site-directed mutagenesis using two single-primer reactions in parallel to generate mutants for protein structure-function studies. *BMC Biotechnol.* **9**:61. <https://doi.org/10.1186/1472-6750-9-61>.
- Finkelstein, R.R., and Lynch, T.J. (2000). The *Arabidopsis* abscisic acid response gene ABI5 encodes a basic leucine zipper transcription factor. *Plant Cell* **12**:599–609. <https://doi.org/10.2307/3871072>.
- Frisch, M.J., Trucks, G.W., Schlegel, J., Scuseria, G.E., Robb, M.A., Cheeseman, J.R., Schlegel, H.B., Scalmani, G., Barone, V., and Mennucci, B. (2013). Gaussian 09, Revision E (Gaussian Inc.).
- Gao, S., Gao, J., Zhu, X., Song, Y., Li, Z., Ren, G., Zhou, X., and Kuai, B. (2016a). ABF2, ABF3, and ABF4 promote ABA-mediated chlorophyll degradation and leaf senescence by transcriptional activation of chlorophyll catabolic genes and senescence-associated genes in *Arabidopsis*. *Mol. Plant* **9**:1272–1285. <https://doi.org/10.1016/j.molp.2016.06.006>.
- Gao, X., Chen, J., Dai, X., Zhang, D., and Zhao, Y. (2016b). An effective strategy for reliably isolating heritable and cas9-free *Arabidopsis* mutants generated by CRISPR/Cas9-mediated genome editing. *Plant Physiol* **171**:1794–1800. <https://doi.org/10.1104/pp.16.00663>.
- Geu-Flores, F., Møldrup, M.E., Böttcher, C., Olsen, C.E., Scheel, D., and Halkier, B.A. (2011). Cytosolic γ -glutamyl peptidases process glutathione conjugates in the biosynthesis of glucosinolates and camalexin in *Arabidopsis*. *Plant Cell* **23**:2456–2469. <https://doi.org/10.1105/tpc.111.083998>.
- Hirai, N., Kondo, S., and Ohigashi, H. (2003). Deuterium-labeled phaseic acid and dihydrophaseic acids for internal standards. *Biosci. Biotechnol. Biochem.* **67**:2408–2415. <https://doi.org/10.1271/bbb.67.2408>.
- Jefferson, R.A., Kavanagh, T.A., and Bevan, M.W. (1987). GUS fusions: beta-glucuronidase as a sensitive and versatile gene fusion marker in higher plants. *EMBO J.* **6**:3901–3907. <https://doi.org/10.1002/j.1460-2075.1987.tb02730.x>.
- Kim, D., Paggi, J.M., Park, C., Bennett, C., and Salzberg, S.L. (2019). Graph-based genome alignment and genotyping with HISAT2 and HISAT-genotype. *Nat. Biotechnol.* **37**:907–915. <https://doi.org/10.1038/s41587-019-0201-4>.
- Kushiro, T., Okamoto, M.K., Nakabayashi, K., Kitamura, S., Asami, T., Hirai, N., Koshiya, T., Kamiya, Y., and Nambara, E. (2004). The *Arabidopsis* cytochrome P450 CYP707A encodes ABA 8'-hydroxylases: key enzymes in ABA catabolism. *EMBO J.* **23**:1647–1656. <https://doi.org/10.1038/sj.emboj.7600121>.
- Liao, Y., Smyth, G.K., and Shi, W. (2014). featureCounts: an efficient general purpose program for assigning sequence reads to genomic features. *Bioinformatics* **30**:923–930. <https://doi.org/10.1093/bioinformatics/btt656>.
- Love, M.I., Huber, W., and Anders, S. (2014). Moderated estimation of fold change and dispersion for RNA-seq data with DESeq2. *Genome Biol* **15**:550. <https://doi.org/10.1186/s13059-014-0550-8>.
- Loveys, B.R., and Milborrow, B.V. (1981). Isolation and characterization of 1'-O-abscisic acid- β -D-glucopyranoside from vegetative tomato tissue. *Aust. J. Plant Physiol.* **8**:571–589. <https://doi.org/10.1071/pp9810571>.
- Lu, T. (2020). Molclus Program. Version 1.9.4. <http://www.keinsci.com/research/molclus.html>.
- Marenich, A.V., Cramer, C.J., and Truhlar, D.G. (2009). Universal solvation model based on solute electron density and on a continuum model of the solvent defined by the bulk dielectric constant and atomic surface tensions. *J. Phys. Chem. B* **113**:6378–6396. <https://doi.org/10.1021/jp810292n>.
- Merilo, E., Jalakas, P., Laanemets, K., Mohammadi, O., Hõrak, H., Kollist, H., and Brosché, M. (2015). Abscisic acid transport and homeostasis in the context of stomatal regulation. *Mol. Plant* **8**:1321–1333. <https://doi.org/10.1016/j.molp.2015.06.006>.
- Milborrow, B.V. (1969). Identification of "Metabolite C" from abscisic acid and a new structure for phaseic acid. *Chem. Commun.* **71**:966–967.
- Mizutani, M., and Todoroki, Y. (2006). ABA 8'-hydroxylase and its chemical inhibitors. *Phytochem. Rev.* **5**:385–404. <https://doi.org/10.1007/s11101-006-9012-6>.

- Nambara, E., and Marionpoll, A.** (2005). Abscisic acid biosynthesis and catabolism. *Annu. Rev. Plant Biol.* **56**:165–185. <https://doi.org/10.1146/annurev.arplant.56.032604.144046>.
- Neese, F.** (2018). Software update: the ORCA program system, version 4.0. *Wiley Interdiscip. Rev. Comput. Mol. Sci.* **8**:e1327. <https://doi.org/10.1002/wcms.2018.8.issue-110.1002/wcms.1327>.
- Neese, F.** (2012). The ORCA program system. *Wiley Interdiscip. Rev. Comput. Mol. Sci.* **2**:73–78. <https://doi.org/10.1002/wcms.81>.
- Shu, K., Liu, X.-D., Xie, Q., and He, Z.-H.** (2016). Two faces of one seed: hormonal regulation of dormancy and germination. *Mol. Plant* **9**:34–45. <https://doi.org/10.1016/j.molp.2015.08.010>.
- Turečková, V., Novák, O., and Strnad, M.** (2009). Profiling ABA metabolites in *Nicotiana tabacum* L. leaves by ultra-performance liquid chromatography-electrospray tandem mass spectrometry. *Talanta* **80**:390–399. <https://doi.org/10.1016/j.talanta.2009.06.027>.
- Vishwakarma, K., Upadhyay, N., Kumar, N., Yadav, G., Singh, J., Mishra, R.K., Kumar, V., Verma, R., Upadhyay, R.G., Pandey, M., et al.** (2017). Abscisic acid signaling and abiotic stress tolerance in plants: a review on current knowledge and future prospects. *Front. Plant Sci.* **08**:161. <https://doi.org/10.3389/fpls.2017.00161>.
- Vrakas, D., Panderi, I., Hadjipavlou-Litina, D., and Tsantili-Kakoulidou, A.** (2005). Investigation of the relationships between logP and various chromatographic indices for a series of substituted coumarins. Evaluation of their similarity/dissimilarity using multivariate statistics. *QSAR Comb. Sci.* **24**:254–260. <https://doi.org/10.1002/qsar.200430898>.
- Weng, J.-K., Ye, M., Li, B., and Noel, J.P.** (2016). Co-evolution of hormone metabolism and signaling networks expands plant adaptive plasticity. *Cell* **166**:881–893. <https://doi.org/10.1016/j.cell.2016.06.027>.
- Yamaguchi-Shinozaki, K., and Shinozaki, K.** (1994). A novel cis-acting element in an *Arabidopsis* gene is involved in responsiveness to drought, low-temperature, or high-salt stress. *Plant Cell* **6**:251–264. <https://doi.org/10.2307/3869643>.
- Yin, X., Bai, Y.-L., Ye, T., Yu, M., Wu, Y., and Feng, Y.-Q.** (2022). Cinnamoyl coA:NADP oxidoreductase like 1 regulates abscisic acid response by modulating phaseic acid homeostasis in *Arabidopsis thaliana*. *J. Exp. Bot.* **73**:860–872. <https://doi.org/10.1093/jxb/erab474>.
- Yin, X., Liu, X., Xu, B., Lu, P., Dong, T., Yang, D., Ye, T., Feng, Y.Q., and Wu, Y.** (2019). OsMADS18, a membrane-bound MADS-box transcription factor, modulates plant architecture and the abscisic acid response in rice. *J. Exp. Bot.* **70**:3895–3909. <https://doi.org/10.1093/jxb/erz198>.
- Yoo, S.D., Cho, Y.H., and Sheen, J.** (2007). *Arabidopsis* mesophyll protoplasts: a versatile cell system for transient gene expression analysis. *Nat. Protoc.* **2**:1565–1572. <https://doi.org/10.1038/nprot.2007.199>.
- Yu, L., Ye, T., Bai, Y.-L., Cai, W.J., Ding, J., Yuan, B.-F., and Feng, Y.-Q.** (2018). Profiling of potential brassinosteroids in different tissues of rape flower by stable isotope labeling - liquid chromatography/mass spectrometry analysis. *Anal. Chim. Acta* **1037**:55–62. <https://doi.org/10.1016/j.aca.2017.08.038>.
- Zeevaert, J.A.D., and Milborrow, B.V.** (1976). Metabolism of abscisic acid and the occurrence of epidihydrophaseic acid in *Phaseolus vulgaris*. *Phytochemistry* **15**:493–500.
- Zhao, S., Wu, Y., He, Y., Wang, Y., Xiao, J., Li, L., Wang, Y., Chen, X., Xiong, W., and Wu, Y.** (2015). RopGEF2 is involved in ABA-suppression of seed germination and post-germination growth of *Arabidopsis*. *Plant J.* **84**:886–899. <https://doi.org/10.1111/tpj.13046>.
- Zhou, R., Cutler, A.J., Ambrose, S.J., Galka, M.M., Nelson, K.M., Squires, T.M., Loewen, M.K., Jadhav, A.S., Ross, A.R., Taylor, D.C., et al.** (2004). A new abscisic acid catabolic pathway. *Plant Physiol* **134**:361–369. <https://doi.org/10.1104/pp.103.030734>.